# Structure-dynamics relationship in coherent transport through disordered systems

Stefano Mostarda, Federico Levi, Diego Prada-Gracia, Florian Mintert,* and Francesco Rao†

*Freiburg Institute for Advanced Studies, School of Soft Matter Research, Freiburg im Breisgau, Germany.*

Quantum transport is strongly influenced by interference with phase relations that depend sensitively on the scattering medium. Since even small changes in the geometry of the medium can turn constructive interference to destructive, a clear relation between structure and fast, efficient transport is difficult to identify. Here, we present a complex network analysis of quantum transport through disordered systems to elucidate the relationship between transport efficiency and structural organization. Evidence is provided for the emergence of structural classes with different geometries but similar high efficiency. In particular, we found a clear structural motif that renders transport properties robust against perturbations. Our results pave the way for a systematic rationalization of the design principles behind highly efficient transport which is of paramount importance for technological applications based on non-trivial quantum phenomena.

Transport of charge or energy through disordered landscapes is one of the most exciting mechanisms underlying biological and technological functionality [1–3]. If the entities that are being transported behave wave-like, *i.e.* propagate coherently, interference resulting from scattering off the disordered medium can result in strong focusing behavior due to constructive interference, as observed for example for an electron gas [4], the coherent backscattering of light from atomic clouds [5] and predicted for Bose-Einstein condensates [6]. When this focus lies in the region to which an object should be transmitted, coherent behavior results in enhanced transport as compared to incoherent (particle like) processes [7, 8]. Consequently, it would be highly desirable to exploit such enhanced transport mechanisms.

Constructive interference, however, relies on well-defined phase relations that need to be satisfied rather accurately, relations which get easily altered due to small changes in the geometry of the scattering medium. The onset of destructive interference then reduces transport, or suppresses it completely [9]. This results in a highly complicated structure-functionality relationship: two structures with hardly noticeable geometric differences can lead to strongly different transport properties and two structures with similar transport potential might not share any geometric similarity. It is thus rather hard to identify geometric features associated with good transport properties, what would be absolutely necessary for the use of constructive interference as design principle in technological applications.

The inherent complexity of the problem as well as the large number of degrees of freedom involved calls for the application of advanced statistical tools. Inspired by the substantial achievements of network science to elucidate complex systems like for instance economic growth [10], human diseases [11] and organic chemistry [12], our aim is to shed light on the elusive relationship between the structure of disordered media and constructive interference through the application of a network approach.

Specifically, we considered a discrete two-level $N$-body system, whose interactions are described by a tight-binding Hamiltonian

$$H = \sum_{i \neq j}^{N} J \frac{r_0^3}{|\vec{r}_i - \vec{r}_j|^3} \sigma_i^- \sigma_j^+ \ , \tag{1}$$

where $\sigma_i^{-/+}$ describe the annihilation/creation of an excitation at site $i$, and $J$ is the coupling constant. The interaction rate decays cubically with the distance between the sites in accordance with dipole-dipole interaction. Within this model a *structure* is defined by the positions of the $N$ sites. The initially excited site (input) and the output site where the excitation has to be delivered are located at diagonally opposite corners of a cube of side $r_0$, while the remaining $N - 2$ sites are placed at random positions within this cube.

While we looked at systems with $N = 4$, 6 and 8, most of our attention focused on $N = 6$, being the smallest set for which non-trivial behavior emerged. For this case, a large sample of 100 millions random structures was generated. This sample covered the whole spectrum of transport efficiencies $E$, where $E$ is defined as the maximal probability

$$E = \max_{t \in [0,\tau]} |\langle in| e^{iHt} |out \rangle|^2 \tag{2}$$

to find the excitation at the output site $|out\rangle$ within a short time interval after initialization. In order to access fast transport that necessarily needs to result from constructive interference, we chose $\tau = \frac{1}{10} \frac{2\pi\hbar}{J} \frac{r_{in-out}^3}{r_0^3}$, *i.e.* a time-scale that is ten times shorter than the scale associated with direct interaction between input and output sites [13].

Being interested in the characterization of efficient transport, our analysis focused on structures with $E > 0.9$, a property that is satisfied by only 14280 configurations out of the generated $10^8$. From a structural point of view this reduced set is highly *heterogeneous*, meaning that two structures with similar efficiency do not necessarily share any evident common pattern [13]. Such

structural variety hinders a straightforward interpretation of the geometrical features compatible with efficient transport.

To unravel this structure-dynamics relationship, we applied a set of tools based on complex networks originally developed for the characterization of molecular systems [14, 15]. Specifically, these methods are designed to analyze large ensembles of configurations, potentially allowing in this case a systematic classification of structures which lead to exceptional transport. We generated a complex network where the 14280 structures with $E > 0.9$ represent the nodes and a link is placed between them if two structures are geometrically similar independently on the specific dynamics of the excitation. The parameter used to estimate structural similarity is $S^2 = \sum_{i=1}^{N} d_i^2/N$, where $d_i$, $i \in \{1, ..., 6\}$ is the distance between corresponding sites in any two structures. Links were placed when $S^2 < 0.0125\ r_0^2$ (see Methods in Supp. Mat. for further details on the network creation protocol). The resulting quantum-structures network is shown in Fig. 1a. In this picture, nodes are proportionally close in space according to the amount of common neighbors. The color coding adopted for this network will be discussed in detail below, anticipating at this stage that the presence of densely connected regions, i.e. clusters of nodes which are highly interconnected among each other, indicates the presence of groups of structures with common geometrical motifs.

We identified these regions using a network clusterization algorithm based on a self-consistency criterion in terms of network random walks [15, 16] (see Methods in Supp. Mat.) that split the network into eight clusters comprised of structures with similar sites arrangements. The eight clusters have very different relative populations, respectively of 73.3%, 9.2%, 4.7%, 3.2%, 2.6%, 1.9%, 1.2%, 1.1%. As such, there is a bias towards certain structure types with respect to others. Cumulatively the eight clusters represent the 97% of the whole sample with an unclassified 3% due to noise (see Fig. 5 in Supp. Mat.).

The detection of eight clusters does not imply the presence of eight distinct dynamical behaviors. We therefore probed transport robustness against random displacements of the individual sites of a structure, with displacements restricted to a cube of side 0.05 $r_0$ centered around the original position of the site. For each structure, $\Delta E_{rand}$ was calculated as the original efficiency minus the average efficiency obtained from 1000 site-randomizations. In this scheme, structures were kept rigid under the assumption that the dynamics occurs on a much faster time scale than low-frequency fluctuations of the entire system (e.g. in the context of biological systems this would be equivalent to large-scale protein breathing). The distributions of $\Delta E_{rand}$ for the eight clusters are shown in Fig. 1b. Strikingly, all points overlapped into three regions that we colored in red, blue
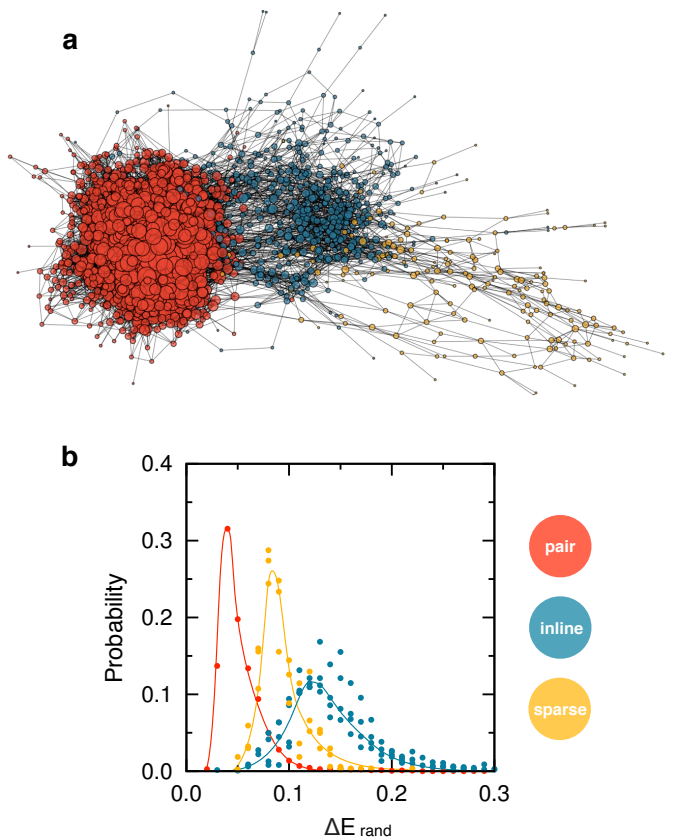


FIG. 1. The quantum-structures network. (a) Nodes in the network represent structures with six excitable sites ($N = 6$) and $E > 0.9$. Links are placed if two structures are geometrically similar. The network layout is obtained via the Fruchterman-Reingold algorithm [17] which puts nodes with several neighbors in common close in space. To avoid overcrowding in the network layout, only 1/5 of the nodes have been represented in the picture. Node size is proportional to the number of links. (b) The probability distribution of efficiency loss upon random displacements for the eight clusters (see text for details). All eight distributions are shown where colors are chosen to highlight the presence of three classes (lines are a guide to the eye). Network nodes color coding follows the class definitions: pair (red), inline (blue) and sparse (yellow).

and yellow. This coding split the network in homogeneously colored parts, as shown in Fig. 1a. This was a-priori not obvious as the network could have shown a certain degree of color mixing, providing strong evidence that network topology and excitation dynamics are correlated properties. Summarizing, the random displacements analysis provided evidence that (i) all structures within a cluster show similar response upon perturbation and (ii) three well-defined types of responses emerge from the eight clusters.

These results suggested a characterization of the whole sample of efficient structures into three classes of similar quantum behavior. The classes are named "pair", "in-
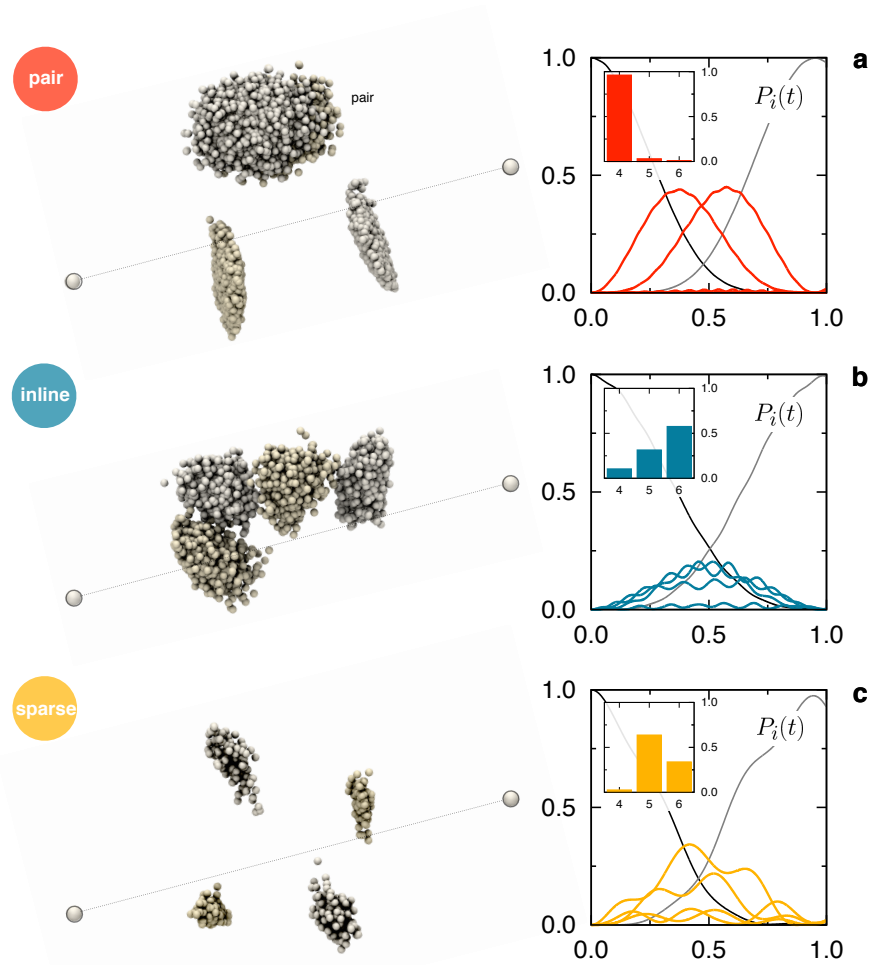
FIG. 2. Structure-dynamics relationship for the (a) pair, (b) inline and (c) sparse classes. On the left side of the figure structures belonging to the cluster containing the most efficient configuration of the class are overimposed (namely cluster number 1, 2 and 7 respectively). Characteristic structural motifs emerge from each of the different clusters (see Supp. Mat. for the superposition procedure). The exciton dynamics of the most efficient structure of each class is shown in the right part of the figure where the x and y-axis represent the time and the excitation probability, respectively. The relative frequencies to find structures with four, five or six active sites within each class are shown as insets (see text). Structural rendering was done with VMD [18].

line" and "sparse" because of their average geometrical properties. In fact, they respectively show couples of sites very close to each other, a compact arrangement around the input/output axis and a more sparse geometry. In terms of clusters, the pair class includes only one cluster (the most populated one, 73.3% of the whole sample) while the inline includes four clusters (17.6%) and the sparse only three (6.3%).

The pair class is very robust against random displacements, with an average loss of efficiency of around 0.06 (red data in Fig. 1b). Interestingly, this class performed much better than the inline and sparse classes which showed an average loss of 0.14 and 0.10, respectively (with losses up to 0.3 for the former). These results indicated that the geometry in these latter classes is more correlated while in the pair class sites can be moved by small displacements in an independent fashion. However, robustness comes with a price: the pair class is generally slower. Taking as reference the time at which the maximum in the output site is reached, the fastest processes for the pair, inline and sparse classes occur within 0.67, 0.30 and 0.54 $\tau$, respectively. This pattern is also reflected in the average speeds, with values of 0.92, 0.83 and 0.86 $\tau$, respectively.

In Fig. 2 several properties of the three classes are illustrated. On the left side of the picture structures belonging to the cluster with highest efficiency within the class are overimposed on top of each other. This repre-

FIG. 4. The most efficient structures in the case $N = 4$ ($E = 0.922$), $N = 6$ ($E = 0.998$) and $N = 8$ ($E = 0.993$). They are shown in light blue, gray and light green, respectively. The gray area highlights the presence of pairs for $N = 6$ and $N = 8$.
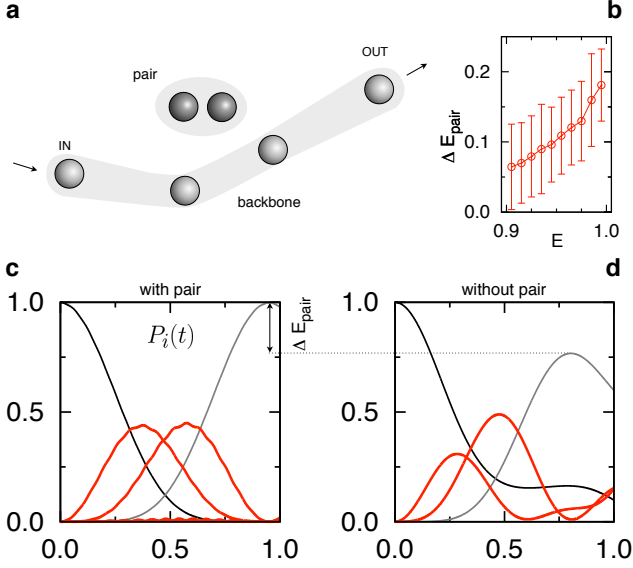
FIG. 3. Characterization of the pair class. (a) The most efficient structure: pair and backbone sites are shown in dark and light gray, respectively. (b) Efficiency loss upon pair removal as a function of the original efficiency $E$. Error bars are calculated according to the standard deviation. (c-d) Comparison of the typical dynamics with and without the pairs. Coherent signal does not focus in the output site in the absence of the pair sites, resulting in an efficiency loss $\Delta E_{pair}$ of up to 0.32 (in the plot the dynamics of the most efficient structure is shown, with $\Delta E_{pair} = 0.23$).

sentation allows a visual appreciation of the structural homogeneity within a cluster as well as of the diversity among clusters. In the right part of the picture, the exciton dynamics of the most efficient structure of the class is shown. In all three cases transport efficiency is larger than 0.97. However, the three dynamics differs substantially. In the pair class (right part of Fig. 2a), two of the intermediate sites are successively excited with no active role of the remaining other sites (excluding input and output). Conversely, the other two classes show more complex patterns of excitation. These results provide evidence for a strong structure-dynamics relationship given that the final values of the efficiency are very similar in all three cases. Hence, structures differing from a geometrical point of view provide distinct exciton dynamics.

As said, the pair class shows a prototypical modular structure. The first module is comprised of four sites including the input and output approximately lined up along the input/output axis, defining a *backbone* for the entire structure (light gray spheres in Fig. 3a). The second module is formed by the remaining two sites, the *pair* (dark gray spheres). Backbone sites are approximately equally spaced between input and output with typical inter-sites distances of around $0.60 - 0.64$ $r_0$. Pair sites instead are always very close to each other with a inter-site distance of around $0.25$ $r_0$ (see Fig. 6 in Supp. Mat.).
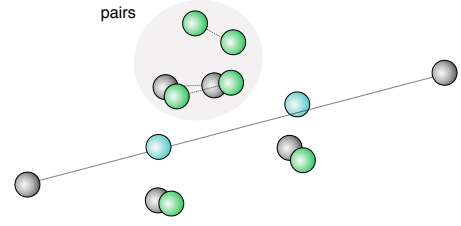
The position of the pair within the box is more heterogeneous than the backbone sites, i.e. their position in space changes between structures as indicated by the disperse cloud of sites in the structural overlaps of Fig. 2a. This property is connected to the exceptional robustness of this class upon random displacements of sites. The pair is usually found in a central position with a relative displacement with respect to the input-output axis. Backbone and pair sites show a completely different dynamical behavior. Systematic analysis of the distribution of the maximum excitations per site within the pair class (excluding input and output sites) revealed that backbone and pair sites can be clearly divided into "active" and "inactive" exciton carriers, respectively (see Fig. 7 in Supp. Mat.). In fact, backbone sites present maximum excitation probabilities always larger than 0.25 while pair sites got never excited more than 0.075 in 99% of the cases.

Strikingly, removal of the pair from the original structures resulted in a systematic efficiency loss of up to 0.32, which is rather surprising given that pairs hardly serve as carrier of the excitation. Efficiency loss is particularly severe for the most efficient realizations due to the sensitivity of perfect constructive interference against perturbations (Fig. 3b). Pair removal affects exciton transport in non-trivial ways as shown by the quantum dynamics of the most efficient structure before and after pair-removal (see Fig. 3c-d). In the modified structure, we found unbalanced transport along backbone sites contrary to what was originally observed as well as an inability of the input site to promptly transmit the excitation to the closest backbone site.

From a geometrical point of view the pair class provides attributes commonly observed in models with different number of sites. For $N = 4$ the ensemble of structures with $E > 0.9$ organized on a line with inter-site spacings very similar to the ones found in the backbone of the pair class. This is shown in Fig. 4 by superimposing the most efficient structures for $N = 4$ and $N = 6$ (light blue and gray spheres, respectively). However, the maximum efficiency for $N = 4$ is of only 0.922 while the presence

of pair sites lead to a maximum efficiency of 0.998 which is also the best value achieved within the whole sample of 100 millions structures. The general role of pairs is confirmed by the $N = 8$ case. In this model roughly half of the whole sample with $E > 0.9$ presented a modular structure with four out of eight sites organized in 2 pairs with the remaining sites perfectly overimposed to the backbone of $N = 6$ (green spheres in Fig. 4). Such geometry clearly represents a generalization of the pair class. Altogether, these results provided strong evidence that pair sites play an important structural role to tune up quantum efficiency, suggesting the idea that they represent a general building strategy towards efficient transport in multi-body quantum systems.

The presence of active and inactive carriers of the transport efficiency in the pair class pointed out a potentially intriguing scheme to rationalize the quantum dynamics of all classes. Taking 0.075 as a threshold to define a site as inactive, the pair class is characterized by a total of four active sites including the input and output (see probability distribution of active sites in the inset of Fig. 2a). However, for the inline and sparse classes no clear separation into number of active sites was found (inset plots in panel b and c of Fig. 2, respectively). Moreover, when this concept was used for the analysis of the efficiency loss upon random displacements by grouping structures according to the number of active sites, ambiguities raised between the five and six active sites groups due to strong overlaps (see Fig. 8 in Supp. Mat.). These results indicated that the active site concept alone is not sufficient to define structural groups with similar dynamics, reiterating the idea that advanced techniques for structural comparisons, like the one performed here, are necessary to unravel the connection between structure and quantum dynamics.

All the presented analysis was performed with perfectly coherent dynamics, but it can be easily extended to models including dephasing (see Supp. Mat. for details). We did so with different dephasing rates, ranging from $0.4/\tau$ to $2.0/\tau$ . Dephasing consistently decreased the efficiency with no specific distinction among the three classes, most importantly without affecting the response-to-noise classification identified with coherent dynamics (see Fig. 9 in Supp. Mat.). The purely destructive effect of dephasing is consistent with the type of analysis performed, which focused on outstandingly fast and efficient transport made possible only by constructive interference.

Our work provided strong evidence for the emergence of non-trivial characteristic structural motifs leading to high quantum transport efficiencies. Specifically, the identification of site pairs not directly participating to the exciton dynamics results in a general strategy to both enhance quantum efficiency and to make structures robust against geometric perturbations. Consequently, a design principle is presented, exploiting enhanced quantum transport in cases where perfect interferometric stability is impossible. Gaining control on this problem is of paramount importance towards the rational design of technologies making use of constructive interference.

## ACKNOWLEDGMENTS

---

* florian.mintert@frias.uni-freiburg.de
† francesco.rao@frias.uni-freiburg.de
[1] G. D. Scholes, G. R. Fleming, A. Olaya-Castro, and R. van Grondelle, Nature chemistry **3**, 763 (Oct. 2011), ISSN 1755-4349, http://www.ncbi.nlm.nih.gov/pubmed/21941248
[2] V. Coropceanu, J. Cornil, D. da Silva Filho, Y. Olivier, R. Silbey, and J. Brédas, Chemical Reviews **107**, 926 (2007)
[3] A. Pivrikas, N. Sariciftci, G. Juška, and R. Österbacka, Progress in Photovoltaics: Research and Applications **15**, 677 (2007)
[4] M. A. Topinka, B. J. LeRoy, R. M. Westervelt, S. E. J. Shaw, R. Fleischmann, E. J. Heller, K. D. Maranowski, and A. C. Gossard, Nature **410**, 183 (2001)
[5] G. Labeyrie, F. de Tomasi, J.-C. Bernard, C. A. Müller, C. Miniatura, and R. Kaiser, Phys. Rev. Lett. **83**, 5266 (Dec 1999), http://link.aps.org/doi/10.1103/PhysRevLett.83.5266
[6] T. Karpiuk, N. Cherroret, K. L. Lee, B. Grémaud, C. A. Müller, and C. Miniatura, Phys. Rev. Lett. **109**, 190601 (Nov 2012), http://link.aps.org/doi/10.1103/PhysRevLett.109.190601
[7] J. Leegwater, The Journal of Physical Chemistry **100**, 14403 (1996)
[8] M. Chachisvilis, O. Kühn, T. Pullerits, and V. Sundström, The Journal of Physical Chemistry B **101**, 7275 (1997)
[9] P. W. Anderson, Phys. Rev. **109**, 1492 (Mar 1958)
[10] C. Hidalgo, B. Klinger, A. Barabási, and R. Hausmann, Science **317**, 482 (2007)
[11] K. Goh, M. Cusick, D. Valle, B. Childs, M. Vidal, and A. Barabási, Proc. Natl. Acad. Sc. USA **104**, 8685 (2007)
[12] B. Grzybowski, K. Bishop, B. Kowalczyk, and C. Wilmer, Nature Chemistry **1**, 31 (2009)
[13] T. Scholak, F. de Melo, T. Wellens, F. Mintert, and A. Buchleitner, Physical Review E **83**, 021912 (2011)
[14] F. Rao and A. Caflisch, J. Mol. Biol. **342**, 299 (2004)
[15] D. Gfeller, P. De Los Rios, A. Caflisch, and F. Rao, Proc. Natl. Acad. Sc. USA **104**, 1817 (2007)
[16] S. Van Dongen, Ph.D. thesis (Univ of Utrecht, Utrecht, The Netherlands).(2000)
[17] T. M. J. Fruchterman and E. M. Reingold, Softw: Pract. Exper. **21**, 1129 (1991)
[18] W. Humphrey, A. Dalke, K. Schulten, *et al.*, Journal of molecular graphics **14**, 33 (1996)

# SUPPLEMENTARY MATERIAL

### Network Creation

Network links are put according to a similarity parameter. The similarity parameter $S$ is calculated as:

$$S^2 = \sum_{i=1}^{n} d_i^2/n \qquad (3)$$

where $d_i$ is the distance between corresponding sites and $i$ runs over all six sites. The sites are indistinguishable, thus all different permutations of the site labels need to be performed (in number of $(N-2)!$, excluding input and output). In addition, symmetry along the in-out axis and an additional mirror symmetry has to be taken into consideration. The measure $S$ between configurations A and B is thus calculated as follows: keeping fixed the set of labels for A, the labels of B are changed. For each of these $(N-2)!$ sets, 180 rotations of 2 degrees each of the configuration B are done around its in-out axis. For each rotation, a mirror reflection relative to the $x-y = 0$ plane is also done. The final value of $S$ is then the minimum value of $\sum_{i=1}^{n} d_i^2/n$ among the $(N-2)! \times 180 \times 2$ possible combinations of labels, rotation and mirror states.

Only $S^2$ values below $0.0125\, r_0^2$ are considered as links in the network. That means, the average $d_i$ between sites of two "superimposed" configurations must be smaller than $\sqrt{0.0125\, r_0^2} \sim 0.11\, r_0$. This value lies just above the tail of the pairwise distance distribution (Fig. 10), being only the most similar structures linked together. Lower values of the cut-off would generate a disconnected network, while values too close to the maximum of the distribution would put links between structures that are not very similar. A double check with another cut-off value of $S^2 < 0.0138\, r_0^2$ was performed, giving results very similar to the ones shown in the main text (see Fig. 8). Although the change from $S^2 < 0.0125\, r_0^2$ to $S^2 < 0.0138\, r_0^2$ seems negligible, it is worth noticing that it corresponds to an increase of the total number of links from $1.03 \cdot 10^6$ to $1.42 \cdot 10^6$, i.e. a conspicuous 40%.

### Clusterization Procedure

In order to obtain different homogeneous classes of configurations, the Markov cluster algorithm (MCL) was used [15, 16]. This algorithm is based on the behavior of random walks on the network and consists of four steps:

*(i)* start with the transition matrix $A$ of the network, where each column is normalized to 1; *(ii)* compute $A^2$; *(iii)* take the $p$th power ($p > 1$) of every element of $A^2$, normalizing afterward each column and *(iv)* go back to step *ii*. After some iterations MCL converges to $A_{MCL}$, where only few entries for each column are non-zero (exactly only one non-zero entry per column). These entries give the clusters. The parameter $p$ is related to the granularity of the clustering process. High values of $p$ generate several small homogeneous clusters. On the other hand, in the limit of $p = 1$, only one cluster is detected. In this work $p = 1.4$, giving a very good signal-to-noise ratio (see Fig. 5 Supp. Mat.). Smaller values of $p$ give similar results. For instance, $p = 1.2$ splits the network into two clusters: the one corresponding to the "pair" class described in the main text and the remaining two classes all together. This suggests that differences between the clusters in "inline" and "sparse" classes appear at a finer degree of granularity, while separation between these and the "pair" class is more evident, requiring a lower parameter $p$ to be resolved.

### Structural superposition

Figures 2 and 11 are obtained as follows: for each cluster, the most connected structure is taken as reference and all the others are superimposed to that: for each of them the combination of labeling, rotation and mirror state which minimizes the similarity parameter $S$ was taken (see Network Creation section). In order to reduce noise, the coordinates of the sites were averaged with the ones from two other structures of the cluster taken at random. Structural rendering was done with VMD [18].

### Dephasing Dynamics

Loss of coherence in the system is introduced via the addition of an incoherent term to the dynamics of the quantum state. We consider an isotropic single body Markovian dephasing. The evolution of the quantum state in time is given by the Lindblad equation

$$\frac{d}{dt}\rho(t) = -i[\rho(t), H] + \gamma\left(\Sigma_z \rho \Sigma_z - \rho\right), \qquad (4)$$

where $\Sigma_z = \sum_i \sigma_z^{(i)}$ and $\sigma_z^{(i)}$ applies the Pauli matrix $\sigma_z$ on the $i$-th site leaving the remaining unperturbed.
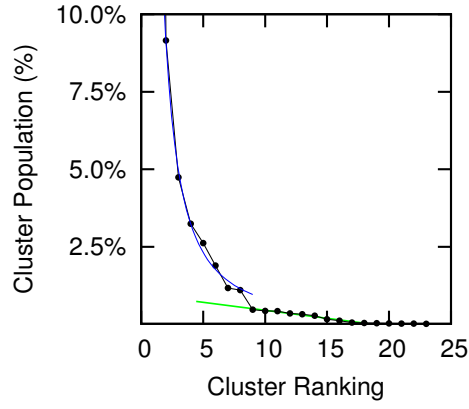
FIG. 5. Cluster populations. The populations of the clusters from 2 to 8 are fitted by a power law function (blue line). The first eight clusters represent cumulatively the 97% of the whole sample. The rest of the clusters, here fitted by a green line, are considered as noise.
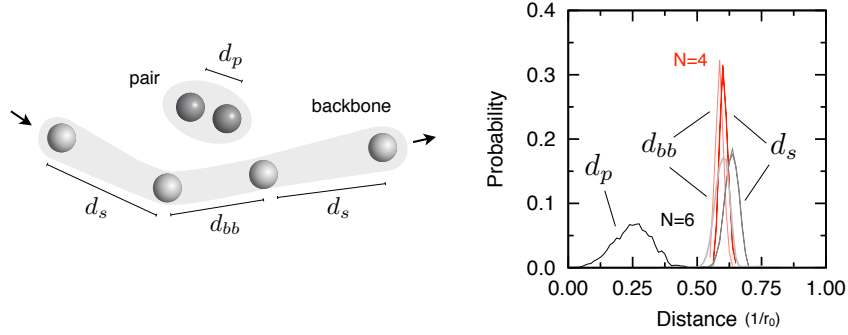


FIG. 6. (left) The most efficient structure of the pair class. (right) Inter-sites distances within the pair class and the $N = 4$ efficient structures are depicted in gray and red, respectively. The distances $d_{bb}$ and $d_s$ show similar distributions in both cases $(0.60 - 0.64 \cdot r_0$ for $N = 6$ and $0.59 - 0.61 \cdot r_0$ for $N = 4)$, revealing a similar backbone geometry, while the intra pair distance $d_p$ is much smaller $(0.25 \cdot r_0)$.
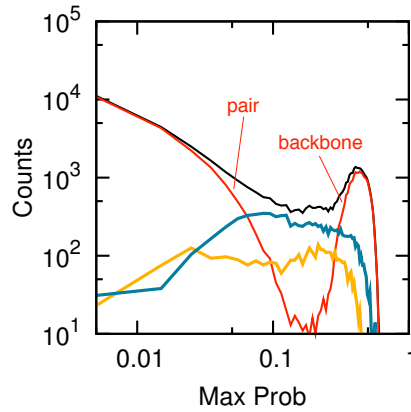


FIG. 7. Distribution of the maximum of the site excitation probability within time $\tau$ (black, in and out sites are not included). The distribution of the pair class reveals two trends (red line): roughly half of the sites never gets excited more than 0.15 (the 99% of which never more than 0.075), the other half has the maximum of excitation above 0.25. The sites belonging to the sparse (yellow) and inline classes (blue) stay in the middle of the distribution with no evident separations.
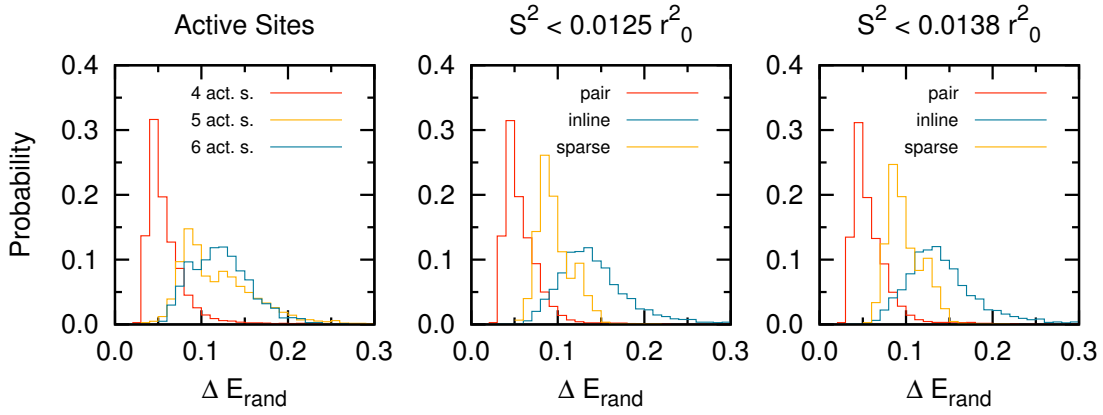
FIG. 8. Efficiency loss upon random displacements (see main text) according to the number of active sites (left) and the class partitioning proposed in this work (center and right). (left) Structures with 4,5 and 6 active sites are shown in red, yellow and blue respectively. This classification is not able to resolve the three different responses to noise presented in Fig. 1b of the main text (reproposed here and grouped by classes for comparison, center). Increasing the number of links of the network by a ~ 40% does not affect the behavior (right), suggesting our results are robust for different values of the similarity cutoff (see also Fig. 10).
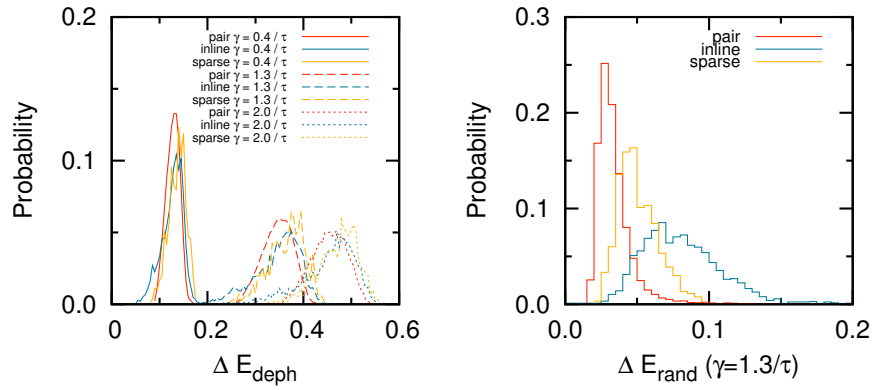


FIG. 9. Efficiency loss upon dephasing. (left) The three classes are shown in red, yellow and blue for the "pair", "sparse" and "inline" classes, respectively. Three different values of $\gamma$ were used (0.4, 1.3 and $2.0/\tau$), here presented in solid, dashed and dotted lines, respectively. No evident difference in dephasing response subsisted between the classes. (right) Efficiency loss upon random displacement in the presence of dephasing ($\gamma = 1.3/\tau$).
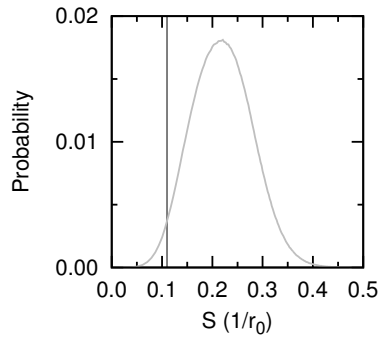


FIG. 10. Pairwise distance distribution between any-two structures for $N = 6$ and $E > 0.9$. The chosen cutoff at $S = 0.11\ r_0$ ($S^2 = 0.0125\ r_0^2$) is shown as a black vertical line.
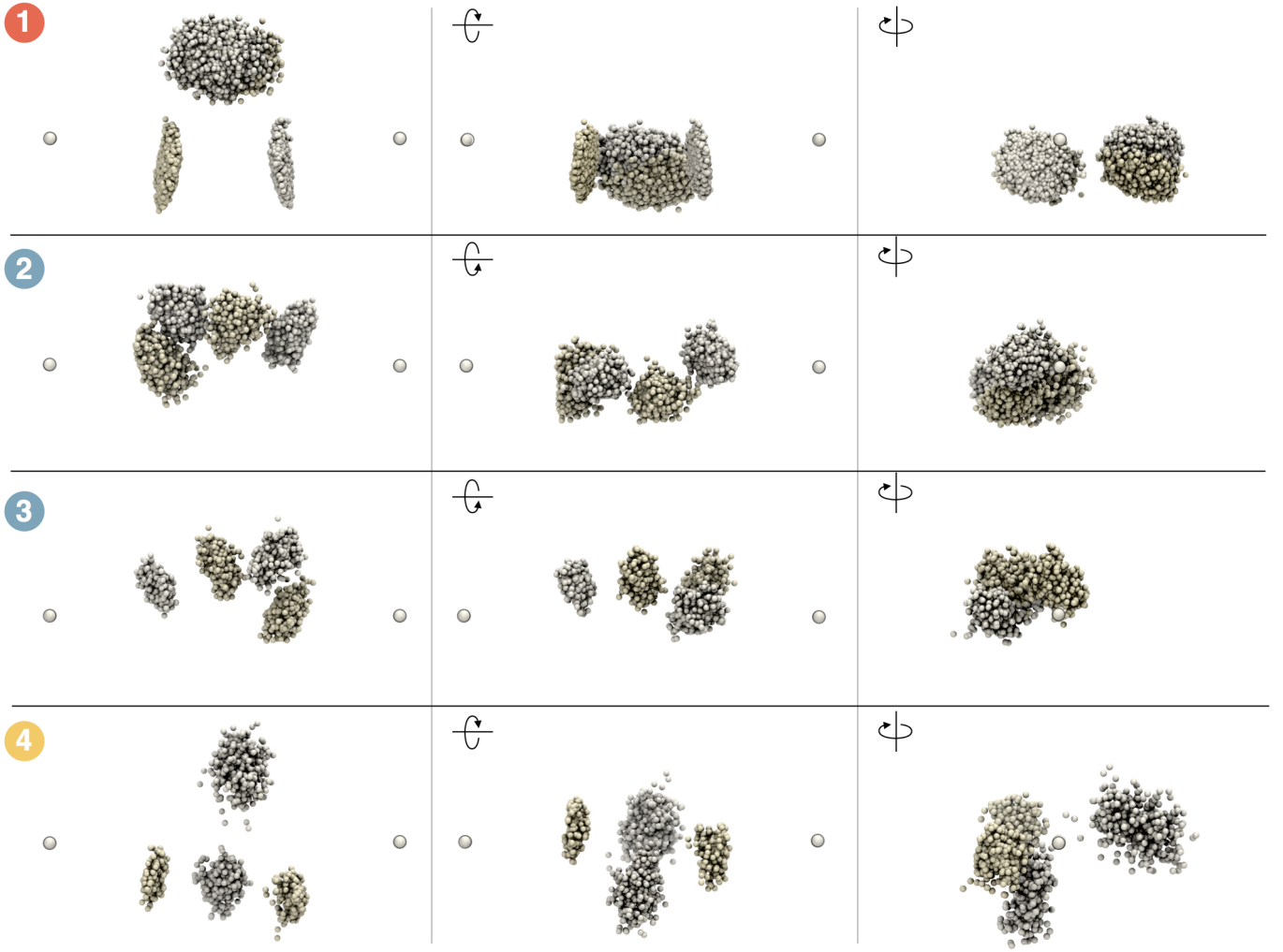
FIG. 11. Superimposition of all structures belonging to clusters 1 to 4. The cluster number is colored according to the class of affiliation (red, blue and yellow for pair, inline and sparse classes, respectively). For clarity, structures are shown in three different orientations.
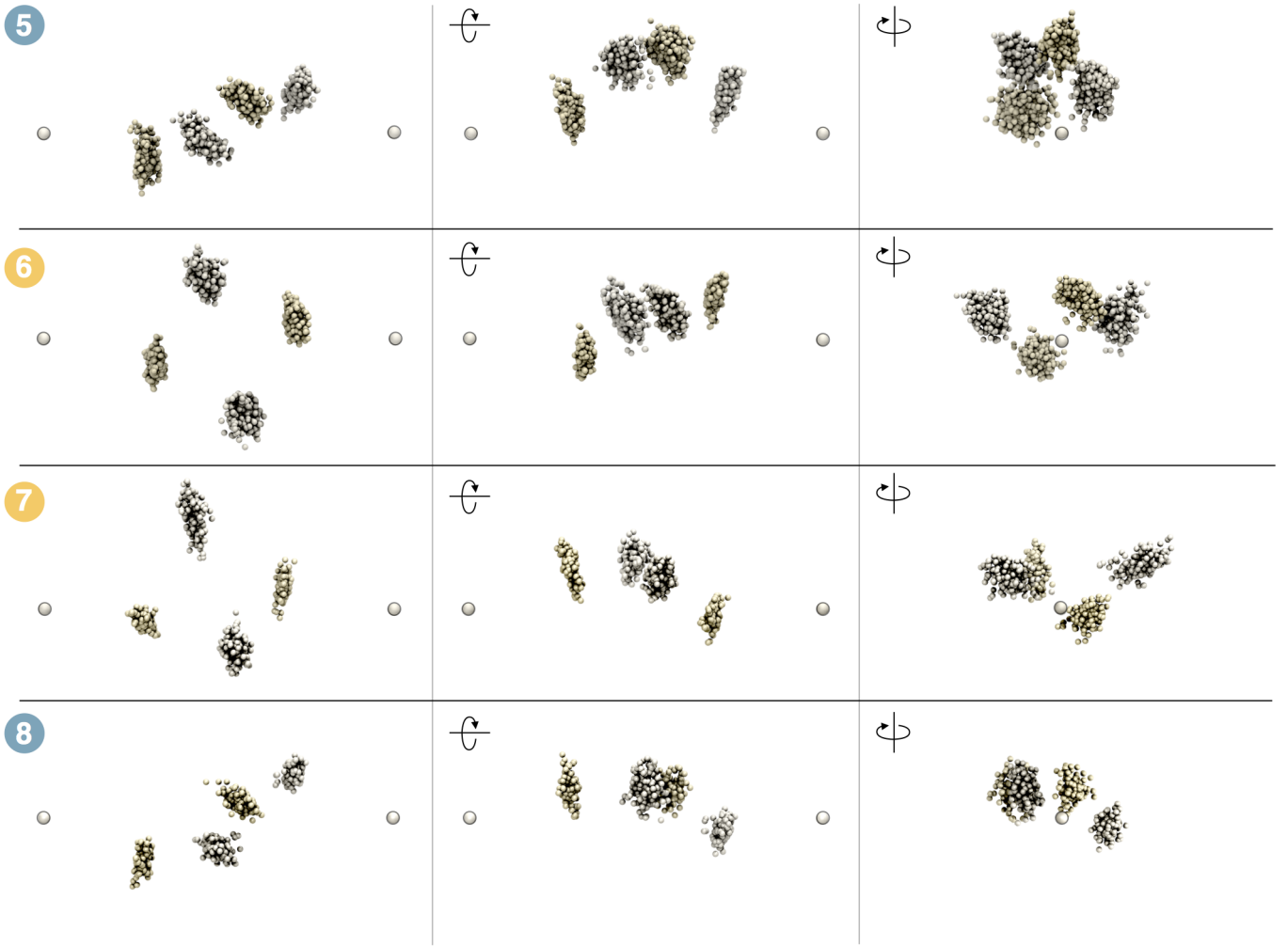
FIG. 11. (continued) Superimposition of all structures belonging to clusters 5 to 8.